Part B: Site-Directed Mutants in a Putative Electron Transfer Pathway from A_0 through A_1 to F_X

Directionality of electron transfer has been a long standing issue in the study of Reaction Centers (see Chapter 2). Spectroscopic indicators can provide conclusive evidence for directional electron transfer in native PS I if the two branches can be distinguished. In the case of bacterial reaction centers the two pheophytins of the L- and M-branch have resolved adsorption lines and can be distinguished optically.

Mutagenesis provides a technique by which the two branches can be rendered distinguishable by introduction of a specific modification into only one branch of cofactors. However, there are a number of important criteria that must be met if this method is to be used beneficially. Firstly, the changes induced by the mutations should be sufficiently subtle that the cells are still able to grow. Secondly, the changes should be localized to the immediate vicinity of the electron transfer cofactors. Otherwise, any correlation between spectroscopic changes and electron transfer along a given branch may be lost. Thirdly, the mutations should not disturb the overall structure and function of all essential functional steps. For example, a mutation that inadvertently alters the directionality of the electron transfer cannot be used to infer this behavior in wild type PS I. Lastly, the mutations should produce changes that are readily characterized using spectroscopic or other techniques.

These considerations led us to approach the problem of distinguishing between the two potential pathways by introducing site-directed mutations in and around the Q_K-A and Q_K-B binding sites and late A_0-A and A_0-B binding sites on the PsaA and PsaB reaction center proteins in *Synechocystis* sp. PCC 6803. Combined with EPR and optical studies of the electron transfer kinetics, a very detailed picture of the influence of the mutations on structure and function can be constructed, which is a prerequisite to uncover the electron transfer pathway in the wild type.

8. Electron Transfer in Cyanobacterial Photosystem I: Spectroscopic Characterization of Site-Directed Mutants in a Putative Electron Transfer Pathway from A_0 through A_1 to F_X

In this chapter the EPR/ENDOR spectroscopic characterization of the following mutants: $W697F_{PsaA}$, $W677F_{PsaB}$, $S692C_{saA}$, $S672C_{PsaB}$, $R694A_{PsaA}$ and $R674A_{PsaB}$ will be presented. These mutants were chosen because they may constitute a potential electron transfer pathway between A_0 and F_X. The results presented here are aimed at gaining an understanding of the physiological and structural changes induced by the mutations. The importance of a detailed characterization is highlighted by the fact that a number of recent papers addressing the issue of directionality in various mutants and PS I preparations using a variety of spectroscopic techniques [34, 89, 90, 91, 92] have reported conflicting evidence compatible with both unidirectional and bi-directional electron transfer. In most of these studies, the directionality is inferred from either optical or EPR/ENDOR spectroscopic properties of modified PS I complexes but little attention has been paid to direct comparison and combined use of optical and EPR/ENDOR data on the same samples and to ensure that the modifications do not alter the structure or function of the quinone. Since it is not possible to do the X-ray structural analysis for all mutants a careful check of all spectroscopic structural indicators characterising the environment of the mutation is a necessary prerequisite to drawing conclusions about the function of the wild type from the function of the mutants.

It will be demonstrated that the mutations described above lead to only subtle changes in the quinone environment and have no perceptible effect on P_{700}. Thus, they are ideally suited to study the directionality of the electron transfer. Moreover, the specific changes in the spectra can be explained satisfactorily in terms of expected changes in the electronic environment the quinone. Together, the results from six different mutants and

several spectroscopic techniques clearly indicate that the quinone detected by CW EPR, transient EPR and ENDOR is located in the PsaA branch of cofactors.

8.1 Rationale for the Choice of the Mutant Strains

Figure 8.1 (top) shows a view (parallel to the membrane plane) of the Q_K-A region of the PsaA subunit and Figure 8.1 (bottom) shows the corresponding view of the Q_K-B region of the PsaB subunit. Examination of this region of the structure reveals a network of contacts between residues extending from $M688_{PsaA}$ ($M668_{PsaB}$), which is the axial ligand to the A_0 Chl eC-A3 (eC-B3), through Q_K-A (Q_K-B) to $G572_{PsaB}$ ($G585_{PsaA}$) in the F_X binding loop, which reaches over from the other subunit of the heterodimer. This continuous set of covalent bonds, ionic contacts, H-bonds and π-π contacts may constitute a highly favourable electron transfer pathway from A_0 through A_1 to F_X. The backbone of $M688_{PsaA}$ ($M668_{PsaB}$) is H-bonded to $S692_{PsaA}$ ($S672_{PsaB}$), which in turn is H-bonded $W697_{PsaA}$ ($W677_{PsaB}$). This Trp is π-stacked with the phylloquinone, which is H-bonded to $L722_{PsaA}$ ($L706_{PsaB}$). In turn, the backbone oxygen of $L722_{PsaA}$ ($L706_{PsaB}$) is H-bonded to the F_X binding loop through $R694_{PsaA}$ ($R674_{PsaB}$), which originates from the start of the respective stromal surface helix jk(1) and acts as a bridge between the return loop containing $L722_{PsaA}$ ($L706_{PsaB}$) and the F_X binding loop provided by the other heterodimeric subunit. Note that for the purpose of the F_X binding this loop of PsaB (PsaA) crosses over into the region occupied below the stromal membrane surface by the other PsaA (PsaB) and establishes the H-bond between $R694_{PsaA}$ ($R674_{PsaB}$) and the backbone oxygen of $G572_{PsaB}$ ($G585_{PsaA}$). This extreme loop crossover is stabilised by intersubunits contacts with PsaC [93]. Additional intra loop contacts stabilize the loop configuration as part of the F_X binding site. When inferring functional properties of the wild type from studies of mutants, it is important to base the conclusions on as many mutants as possible. This is particularly true if it is not known what kind of cofactors structural changes are induced by the mutations.

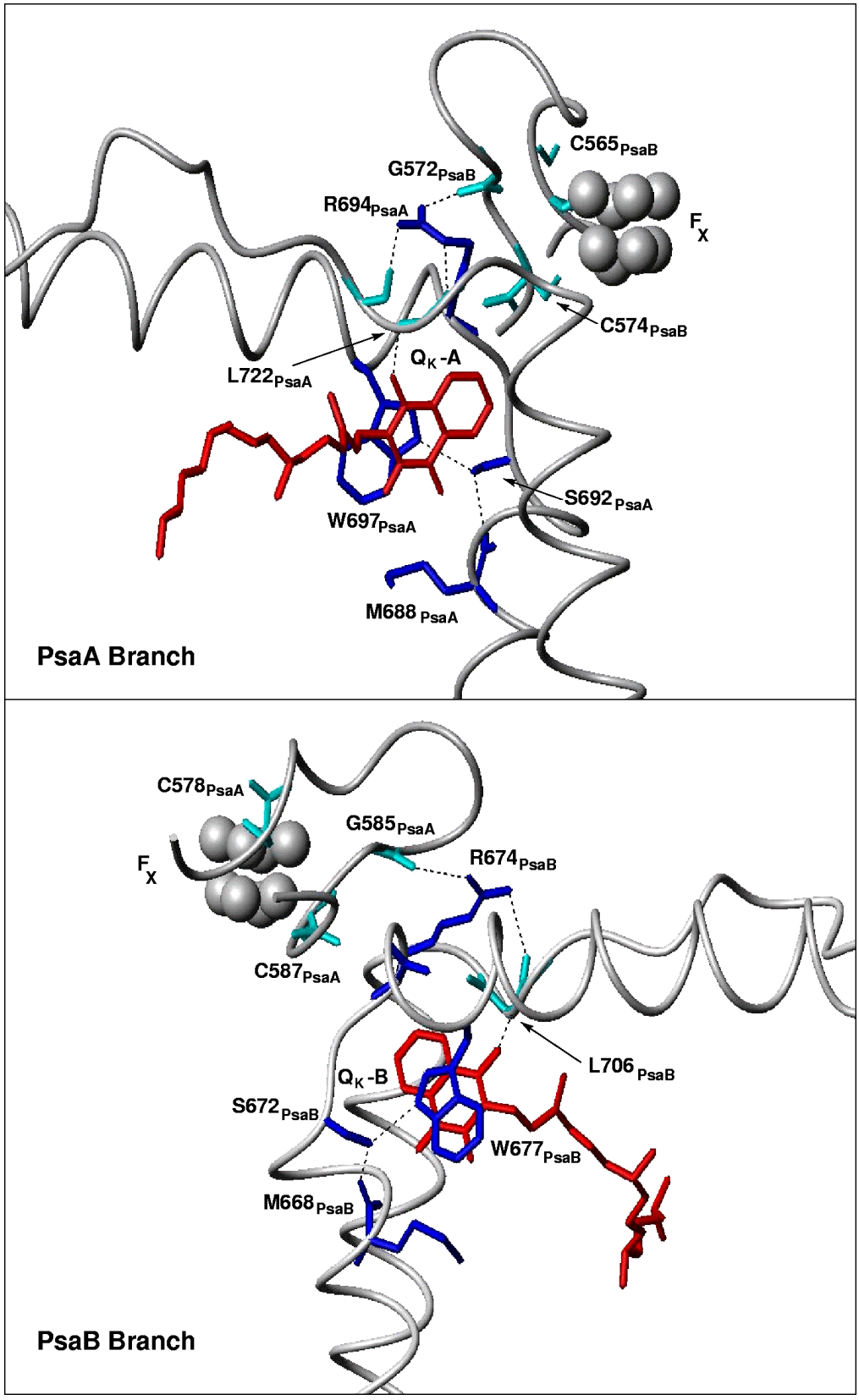

Figure 8.1. Structure environment of the two phylloquinone binding sites in PS I according to the 2.5 Å resolution X-ray structure of PS I [1] (pdb entry 1JB0). The binding sites are viewed from a direction roughly parallel to the membrane plane. Marked are the locations of those amino acids discussed in the text. The figure was constructed using the program MOLMOL.

Immediate candidates for mutation are $W697_{PsaA}$ and $W677_{PsaB}$, which are in π-π contact with Q_K-A and Q_K-B and are therefore likely to influence the redox properties of the quinones. Since we wanted to restrict the influence of the mutations to the vicinity of the amino acids involved, we chose to make a conservative replacement, changing the Trp to a Phe. As can be seen in Figure 8.1 (top), a side chain oxygen of $S692_{PsaA}$ forms a H-bond with the imidazole nitrogen of $W697_{PsaA}$, which is in π–π contact with Q_K-A. The hydrogen atom, which is shared between the Ser and Trp residues, is also close to the carbonyl oxygen ortho to the methyl group on the quinone ring. Thus, the quinone may participate to some extent in the H-bonding, although the distances and angles argue against a significant interaction. Rather, the function of the Ser residue is likely to stabilize the Trp in π–π contact with the quinone. Hence, $S692_{PsaA}$ and $S672_{PsaB}$ were considered further good candidates for mutagenesis. Again, by making a conservative mutation of the Ser to a Cys, we expect only subtle changes in the H-bonding to the neighbouring Trp. Figure 8.1 also highlights the two symmetry-related residues, $R694_{PsaA}$ and $R674_{PsaB}$, which link the A_1 and F_X binding sites as described above. Thus, the $R694_{PsaA}$ and $R674_{PsaB}$ residues were also considered candidates for mutagenesis. Their side chains are close to F_X and positively charged thus exchange of Arg to uncharged side chain can affect the F_X redox potential. The PsaA or PsaB specific mutants $W697F_{PsaA}$, $W677F_{PsaB}$, $S692C_{saA}$, $S672C_{PsaB}$, $R694A_{PsaA}$ and $R674A_{PsaB}$ were therefore constructed, since they would be most likely to show an effect on the acceptors involved in the electron transfer pathways.

8.2 Physiological Characterization of the Mutant Strains [64]

Mutants were generated by Wu Xu at the Iowa University in the group of Professor P. Chitnis. Physiological characterization of the mutant strains has been done at the Pennsylvania State University by group of Professor J. Golbeck. The growth rates of the wild type and mutant strains were compared at different light intensities under photoautotrophic and photomixotrophic growth conditions. All mutant strains grew

photoautotrophically, but they all displayed reduced growth rates compared to the wild type. The growth rates of all of the mutant strains were significantly slower at high light intensities (ca. 250 μmoles m^{-2} s^{-1}) than at low light intensities (ca. 5 μmoles m^{-2} s^{-1}). In contrast, the growth rate of the wild-type strain was marginally faster at high light intensities than at normal light intensities.

When the wild-type and mutant strains were grown photomixotrophically with glucose in the medium, all mutant strains displayed growth rates similar to the wild type. Under these conditions, heterotrophy is the major energy acquisition mode in *Synechocystis* sp. PCC 6803, and respiratory electron transport rates in the mutant strains are deemed sufficient to sustain a normal heterotrophic growth.

To assess the physiological impact of the mutations on the photosynthetic activity, PS I electron throughput was measured either by oxygen uptake using 3,6 diaminodurene as electron donor, and methyl viologen as electron acceptor or by $NADP^+$ reduction using cytochrome c_6 as donor and ferredoxin as acceptor. All mutant strains showed lower levels of PS I-mediated electron transfer activity compared to the wild type. Regardless of whether the mutation was in the Trp, Ser or Arg residues, the electron throughput activities of the PsaA-side mutants were consistently lower than the PsaB-side mutants.

When grown under normal light intensities, the mutant strains contained less chlorophyll than the wild type. In particular, the replacement of the π-stacked Trp with Phe in both the Q_K-A and Q_K-B binding sites has a more pronounced effect on PS I stability than does the alteration of a H-bond to the π-stacked Trp residues or the loss of the H-bond by the replacement of the Arg residues with Ala residues. Note also that whether the mutation was in the Trp, Ser or Arg residues, the chlorophyll content in all of the PsaA-side mutant strains is lower than in the PsaB-side mutant strains. Since PS I is the major chlorophyll-containing complex under iron-replete growth conditions, the lower growth rates may be a function of a lower concentration of PS I in the mutant cells. The data implies that the electron transfer activity in the membranes may be more related to the amount of PS I in the mutant cells as to any direct effect on primary electron transfer. The

lower levels of PS I could be a result of down-regulation in response to low electron transfer efficiency.

PS I mediated electron transfer activity and chlorophyll content of mutant cells always deviated more for the PsaA brunch mutants then for PsaB branch from the WT. This can be conceded as additional, independent support to the biased electron transfer activity along the PsaA branch which will be determined in the following sections and Chapter 9.

8.3 Spin Polarization patterns of $P_{700}^{+}A_1^{-}$ at X-and Q-band

The TR-EPR detected spin polarization pattern of the $P_{700}^{+}A_1^{-}$ state is sensitive to the orientation of A_1 and its environment (see [33] for a recent review). Thus, they provide an appropriate method for probing the structural changes of the mutations using specific structural indicators of the quinone environment. Figure 8.2 shows the direct detected transient X-band, Q-band, and W-band spectra of $P_{700}^{+}A_1^{-}$ in the $W697F_{PsaA}$ and $W677F_{PsaB}$ mutants together with the corresponding wild type spectra taken in frozen solution at low temperature. With the exception of the W-band spectra, the same comparison for $S692C_{PsaA}$ and $S672C_{PsaB}$ is shown in Figure 8.3 and corresponding X-band and Q-band spectra of the $R694A_{PsaA}$ and $R674A_{PsaB}$ mutants are shown in Figure 8.4. The overall polarization patterns for all of the latter two mutants are very similar to the wild type. The effect of the hyperfine couplings is most pronounced in X-band spectra while the g-anisotropy plays the dominant role in the Q-band and W-band spectra, which makes the latter more sensitive to the quinone orientation. With the exception of the $W697F_{PsaA}$ mutant, the Q-band spectra are within S/N identical with the wild type. We conclude that these mutations do not induce any significant change in either the orientation of the observed quinone or in its *g*-anisotropy. In the Q-band spectrum of the $W697F_{PsaA}$ mutant, there may be a small difference with the wild-type in the low field part of the spectrum. Quinone π stacking interaction is known for its influence on the *g*-tensor parameters.

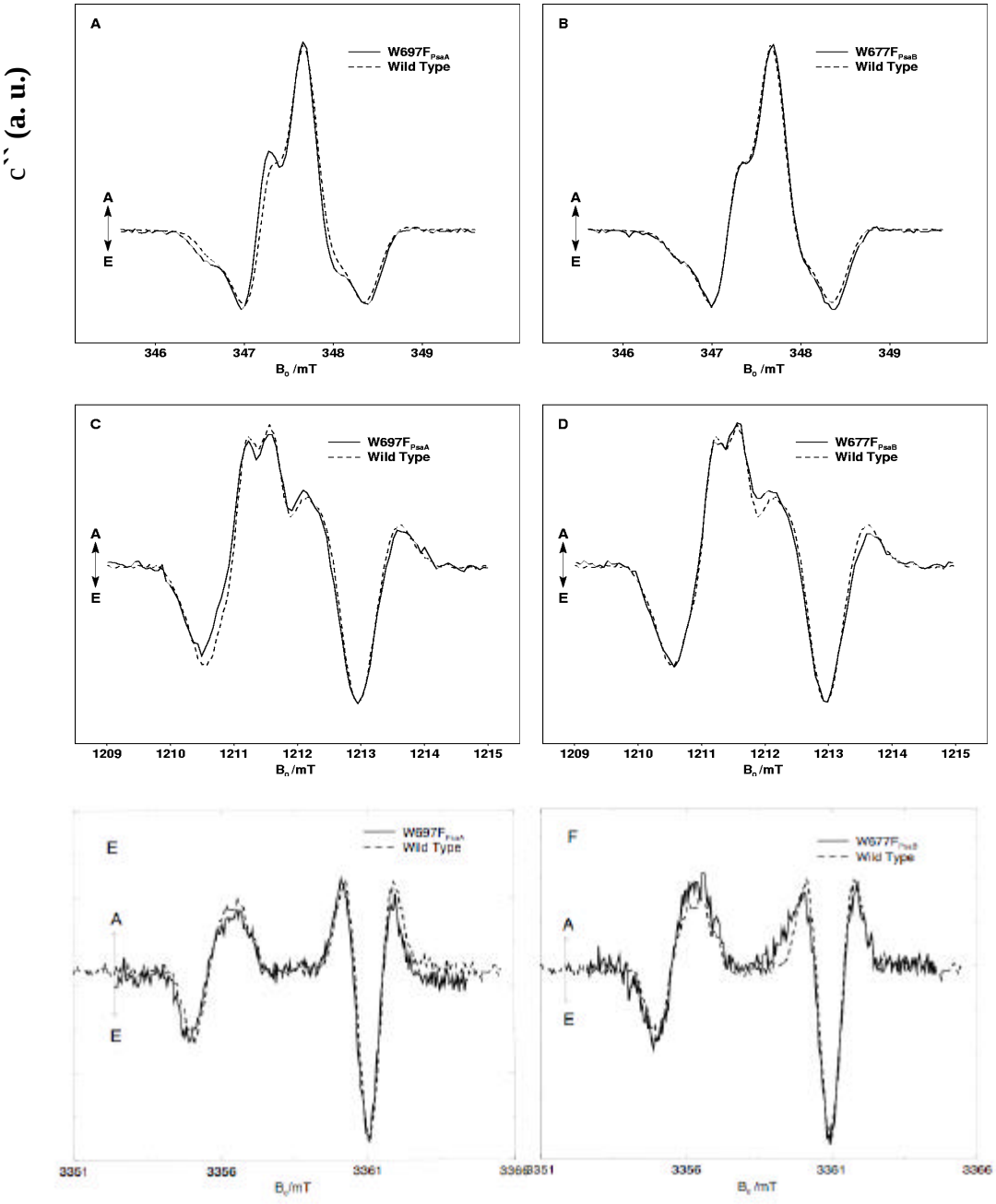

Figure 8.2. X-band (top), Q-band (middle) and W-band (bottom) spin polarized EPR spectra of $P_{700}{}^{+}A_1{}^{-}$ state PS I complexes from the $W697F_{PsaA}$, $W677F_{PsaB}$ mutants (solid spectra) compared with wild type (dashed spectra) at 80 K. The spectra have been extracted from the full time/field datasets by integrating the signal intensity in a time window from 152 ns to 1520 ns following the laser flash. Note that the field axes are different for the X-band and Q-band spectra and that the spectral width at Q-band is much larger. The experimental conditions are given in the Materials and Methods section.

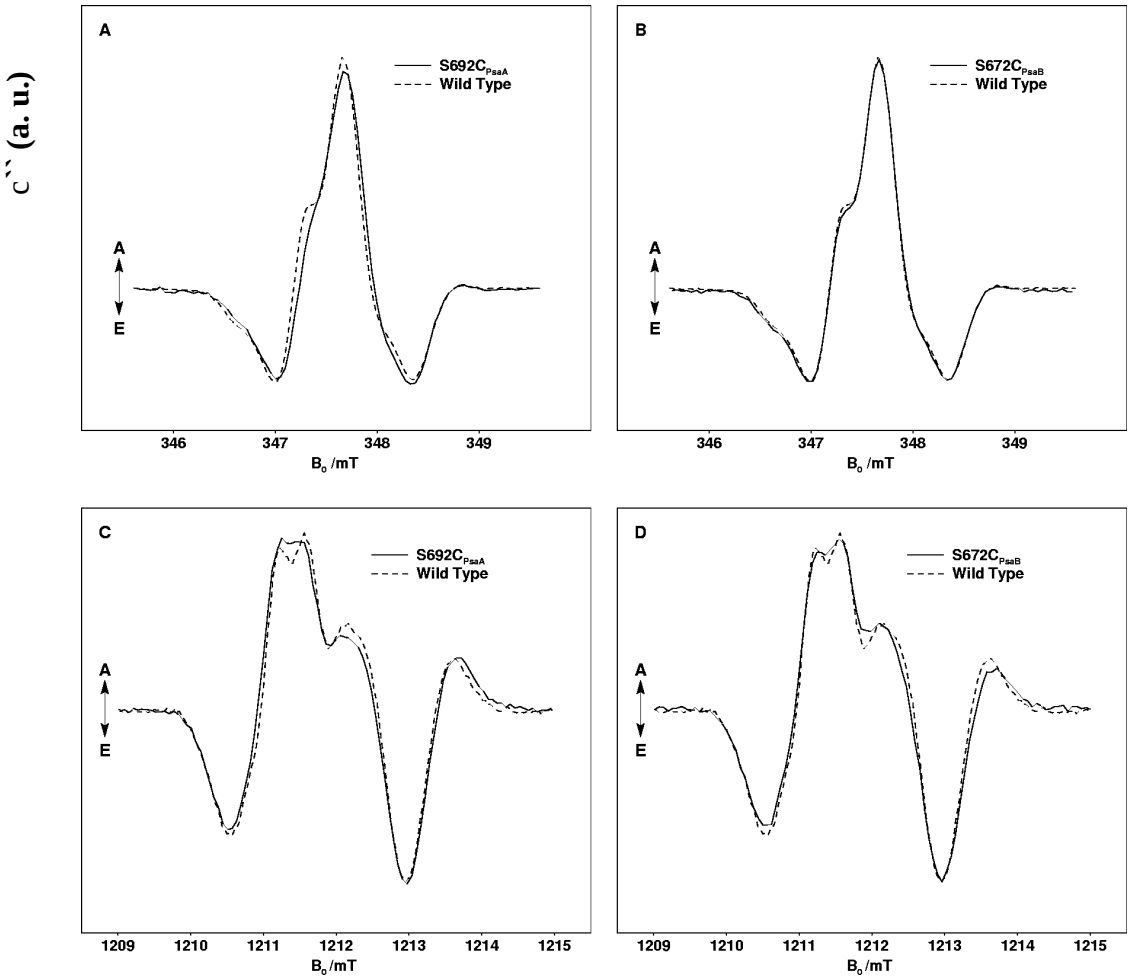

Figure 8.3. X-band (top) and Q-band (bottom) spin polarized EPR spectra of PS I complexes from the S692C$_{PsaA}$, S672C$_{PsaB}$ mutants compared with wild type at 80 K. All other conditions are as for Figure 8.2.

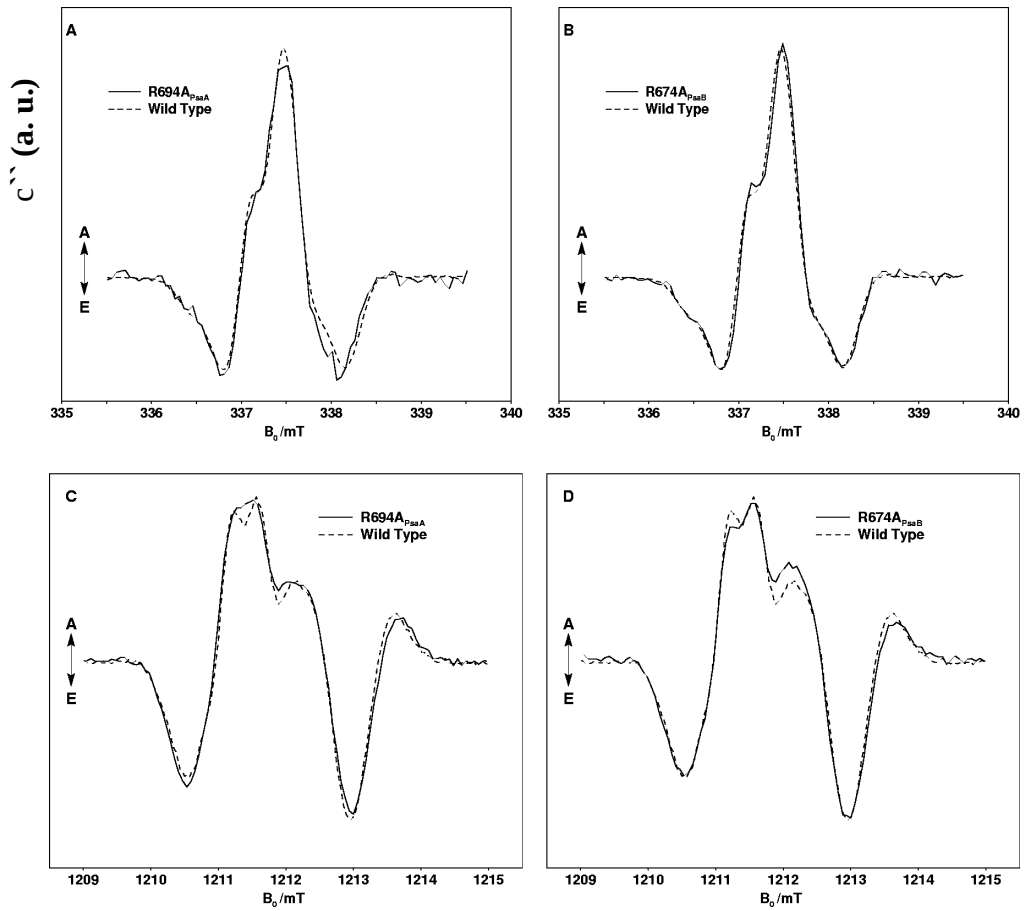

Figure 8.4. X-band (top) and Q-band (bottom) spin polarized EPR spectra of $P_{700}^{+}A_1^{-}$ state of PS I complexes from the $R694A_{PsaA}$ and $R674A_{PsaB}$ mutants compared with wild type (dashed spectra) at 135 K. The spectra are the integrated signal intensity in a time window 0.8-1.6 μs following the laser flash. All other conditions are as for Figure 8.2.

To increase the spectral resolution and to determine the significance of this effect (mainly the difference in the *g*-tensor) we performed studies of the $W697F_{PsaA}$ and $W677F_{PsaB}$ mutants at W-band (95 GHz). As shown in Figure 8.2 (E, F), the PsaB mutant is identical with the wild type, while the PsaA mutant may have a slightly increased *g*-anisotropy: the quinone g_{xx} component shifts to a higher value. However, even with the increased resolution available at W-band, the difference between the mutant and the wild type is quite small. There may be no significant change nether in the *g*-anisotropy, nor in the orientation of the quinone.

More careful inspection of the X-band spectra (Figures 8.2A, 8.2B and 8.3A, 8.3B) shows that while the spectra of the PsaB mutants are almost indistinguishable from those of the wild type, the methyl hyperfine splitting pattern is slightly more pronounced for the $W697F_{PsaA}$ mutant (Figure 8.2A) and less pronounced for the $S692C_{PsaA}$ mutant (Figure 8.3A). This is seen most clearly on the low field shoulder of the central absorptive peak and suggests that the PsaA mutations affect the methyl hyperfine coupling. There is also a slight shift of the low field emission in the Q-band spectrum of the $W697F_{PsaA}$ mutant compared to wild type, which is consistent with an increase in the methyl hyperfine coupling.

8.4 Pulsed ENDOR of $P_{700}^{+}A_1^{-}$

The small effect of the mutations on the resolution of the methyl group hfs observed at X-band motivated us to perform pulsed ENDOR experiments on the $P_{700}^{+}A_1^{-}$ state and quantify this effect for the Trp, Ser and Arg mutants. Figure 8.5 compares the pulsed ENDOR spectra of $P_{700}^{+}A_1^{-}$ in the $W697F_{PsaA}$, $W677F_{PsaB}$, $S692C_{PsaA}$, and $S672C_{PsaB}$ mutants (top) as well as the $R694A_{PsaA}$ and $R674A_{PsaB}$ mutants (bottom). The ENDOR spectra are taken at a field position for which the spectra appear approximately symmetric with respect to the proton Larmor frequency. ENDOR lines occur in absorption (positive features) and emission (negative features) depending on the electron spin polarization of the radical pair (for a detailed analysis see [67]). As for the wild type, two clearly resolved powder patterns of an axially-symmetric tensor are observed on the extremities of the spectra in the range 8.6-10.6 MHz and 18.9-20.9 MHz. These features are assigned to the ring methyl group of phylloquinone. A qualitative comparison shows that the spectra of the PsaB mutants are virtually identical to each other. In addition, the spectra of the PsaB mutants agree well with spectra recorded for wild type PS I from *Synechococcus elongatus*. The spectra of the PsaA mutants display systematic changes.

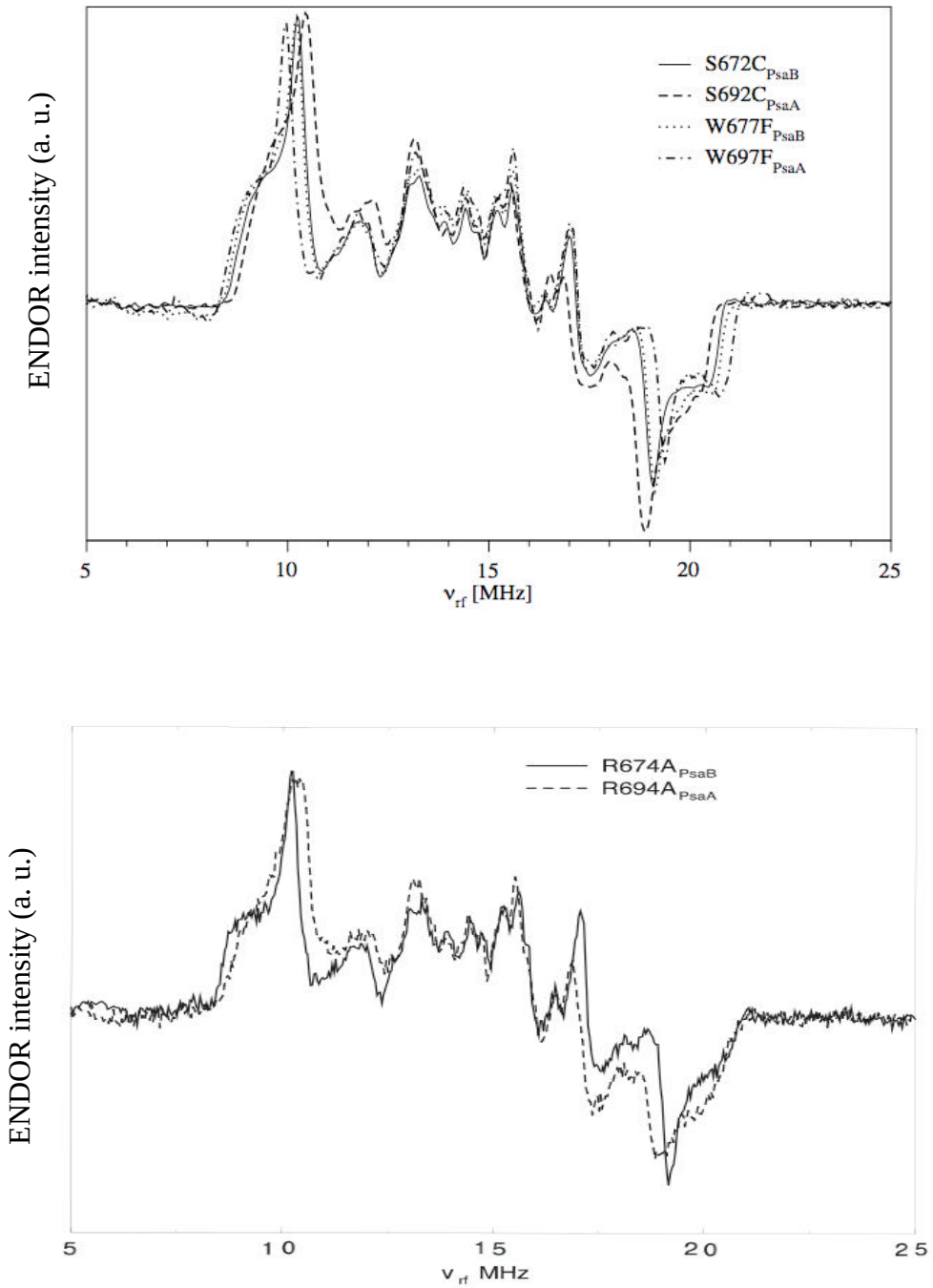

Figure 8.5. Pulsed ENDOR of the $P_{700}^{+}A_1^{-}$ state in PS I point mutants. Top: $S672C_{PsaB}$ (solid line), $S692C_{PsaA}$ (dashed line), $W677F_{PsaB}$ (dotted line), $W697F_{PsaA}$ (dashed-dotted line). Note that the spectra of the B-side mutants coincide very well and represent essentially wild type spectra. Bottom: $R694A_{PsaA}$ (solid line), $R674A_{PsaB}$ (dashed line). See Materials and Methods for details of the pulse sequences and other experimental conditions.

In Figure 8.5 (top), both edges of the methyl hyperfine powder patterns, representing the $A_{\parallel}$ and $A_{\perp}$ hyperfine tensor components, shift within experimental accuracy by the same amount of about 5% for both PsaA mutants, compared to the PsaB mutants. The direction of the shift, however, is opposite in the two cases with larger couplings observed for the $W679F_{PsaA}$ mutant and smaller couplings in the $S692C_{PsaA}$ mutant. Since the $A_{\parallel}$ and $A_{\perp}$ components change simultaneously, the tensor asymmetry does not change but rather the isotropic hyperfine coupling constant, *i.e*. the change is determined by the spin density at the carbon ring position to which the methyl group is attached. Using the hyperfine tensor components of *Synechococcus elongatus* and both PsaB mutants of $A_{\parallel}$=12.13±0.1 MHz, $A_{\perp}$=8.8±0.1 MHz [67], the shifts in the PsaA mutant corresponds to $A_{\parallel}$=11.8±0.1 MHz, $A_{\perp}$=8.3±0.1 MHz for $S692C_{PsaA}$ and $A_{\parallel}$=12.9±0.1 MHz, $A_{\perp}$=9.4±0.1 MHz for $W697F_{PsaA}$. As discussed in Chapter 7 the spin density at the $-CH_3$ position (or A_{iso}) is increased with respect to the average value in isotropic solution. Hence the relative change of the A_{iso} of the Ser and Trp mutants according to the solution situation is almost 20% and has an opposite sign. In addition to these changes in the methyl hyperfine couplings, the $S692C_{PsaA}$ mutant also shows spectral changes compared to the wild type in the 11.5-12.5 MHz and 17.0-18.0 MHz range (Figure 8.5, lower panel). The hyperfine couplings corresponding to the features in these regions of the spectrum are also reduced by about the same amount as the methyl couplings, their assignments to specific protons, however, is not yet certain. Figure 8.5 (bottom) shows that the ENDOR spectrum of the $R674A_{PsaB}$ mutant is again identical to those of the PsaB mutants above (and of wild type (19)). In contrast, the spectrum of the $R694A_{PsaA}$ mutant shows characteristic shifts of relevant spectral features, actually very similar to those observed for the $S692C_{PsaA}$ mutant in Figure 8.5 (top).

Since the EPR observed for the $P_{700}^{+}A_1^{-}$ state represents that of the PsaA side, it is not surprising that spectral changes occur only for the PsaA-side mutant, while the PsaB-side mutation is too distant from the Q_K-A site to show any observable effect. Note that the different results for all the A- and B-side mutants confirm nicely the specificity of each of the mutants. There are no obvious structural hints why the spectral changes for the

$S692C_{PsaA}$ and $R694A_{PsaA}$ mutant should be so similar. On the other hand, the relative changes are quite small (about 5%) but have the same sign. If a reduction in the spin density correlates with a weaker H-bond from the quinone to the back bone Leu, then it might be suggested that a mutation of both the Ser and Arg residues involved in the hydrogen bond network (Figure 8.1) should be noticeable. As a final note, it should be remarked that all the observed changes in the hyperfine parameters for the mutants are most precisely evaluated from the ENDOR data. Nevertheless, they can also be recognised and are consistent with the changes observed in the spin polarization patterns of $P_{700}^{+}A_1^{-}$ (Figures 8.3 and 8.4).

Clearly, only mutations in the PsaA protein lead to a change in the hyperfine couplings while PsaB mutations do not, which shows that only the $P_{700}^{+}A_1^{-}$ state of the PsaA branch is observed in the transient EPR and ENDOR experiments.

Keeping in mind that for the low temperature spin polarization patterns and pulsed ENDOR experiments, only the fraction of reaction centers are observed in which an electron transfer cycle through A_1 takes place, we conclude that for this fraction the electron transfer occurs along the PsaA branch. It is conceivable that the behavior at low temperature might be different from the behavior under physiological conditions. Therefore it is important to combine these experiments with measurements near room temperature, in which forward electron transfer past $P_{700}^{+}A_1^{-}$ is observed.

8.5 Effect of the Mutations on the Spin Density Distribution in the Phylloquinone Molecule.

The interpretation of the spectra assumes that the mutations cause only subtle changes in the properties of the cofactors without altering the electron transfer pathway. Ideally, the physiological properties of the mutants would be identical to the wild type. Although the mutants do not rigorously fulfil this criterion, the differences are sufficiently small, especially for the Ser and Arg mutants [64]. Indeed, the lower growth rate and the lower rates of steady-state PS I-based activity in the membranes correlate with a lower-

than-normal PS I content in the mutant cells. Furthermore, there appears to be no correlation between growth rate and the kinetic data, *i.e.* the rate of oxidation of A_1^-. Because the mechanism, by which the PS I content in the membranes is regulated, is not known in detail, it is difficult to infer whether the lower amount of PS I is a result of poor assembly due to structural changes or of down-regulation of PS I due to impairment of its function. However, the physiological data show that all the perturbations induced by the mutations are minor and are likely not to influence the local A_1 site structure.

The ENDOR and EPR data, on the other hand, give details about the local environment of the cofactors. The small but clearly-visible shifts in the ENDOR spectra and corresponding subtle changes in the EPR spectra show that the mutations of the Q_K-A binding site lead to changes in the spin density distribution on the phylloquinone while at the same time the spin polarization patterns, especially at Q-band, show that none of the mutations affect the quinone position and orientation. Two protein-cofactor interactions are well established to have a significant influence on the spin density distribution: (i) asymmetric H-bonds to the two quinone carbonyl groups as was described in detail earlier and (ii) π-stacking between an aromatic residue and the quinone ring. An interpretation of those changes induced by the mutations in terms of these two interactions can be suggested. However, this interpretation remains preliminary since other factors such as local charges or induced dipoles can also influence the spectral results. In wild type PS I, the single H-bond to $L722_{PsaA}$ (see Figure 8.1, top and Chapters 6, 7) introduces an asymmetric spin density distribution by increasing the spin density at the ring position of the methyl group. The π-stacking arrangement with $W697_{PsaA}$, on the other hand, reduces the effect of the asymmetric H-bonding. In the $W697F_{PsaA}$ mutant it is likely that the π-stacking is weakened so that the distortion of the spin density due to the H-bond to $L722_{PsaA}$ is increased. Consistent with this, the methyl hyperfine couplings are increased in the $W697F_{PsaA}$ mutant. The opposite effect is observed for the $S692C_{PsaA}$ mutant. The change is likely to affect the carbonyl oxygen in the ortho position with respect to the methyl group of the quinone. It may also influence the H-bond network surrounding the quinone site. Although Ser and Cys differ only by the substitution of the hydroxyl group in

serine by a thiol group in cysteine, the van der Waals radius of the sulphur is larger than that of oxygen. The effect of this change on the environment is difficult to predict. The weaker methyl hyperfine coupling in the $S692C_{PsaA}$ mutant is consistent with an increase in the electron withdrawing ability of the surroundings of the carbonyl oxygen ortho to the methyl group.

8.6 PsaA branch is EPR active at low temperature

All data reported here from the point mutants suggest that the quinone measured by EPR and ENDOR is the quinone in the PsaA branch. Photoactivity of mainly the quinone in the PsaA branch has been concluded from the EPR studies of a PsaE/PsaF double deletion mutant [89], which showed selective solvent access to the Q_K-A and correspondingly an inability to photoaccumulate Q_K-A^- and an appearance of only an A_0^- spectrum. The appearance of A_0^- is thought to require a double reduction and protonation of the quinone. At low temperature, the spin polarization patterns and the pulsed ENDOR spectra all show an effect when mutations are made to PsaA but the corresponding spectra from the PsaB mutants are identical to those from wild type. Thus, we conclude that only the phylloquinone bound to PsaA (Q_K-A) contributes to these spectra whereas the phylloquinone bound to PsaB (Q_K-B) does not. Because the observed changes in the properties of the quinone are small, it is reasonable to extrapolate from this result the conclusion that the electron transfer cycle between P_{700} and A_1 measured by EPR at low temperature occurs along the PsaA branch. The same conclusion was reached by Heathcote et al. [91] and by Boudreaux *et al.* [94] from point mutation studies in the eukaryotic organism, *Chlamydomonas reinhardtii*. However, it must be kept in mind that cyclic electron transfer involving P_{700} and A_1 occurs in only a fraction of the RCs in frozen solution, while a stable charge separation to the iron-sulphur clusters takes place in the remainder. Therefore, we also need to consider the pathway taken by the fraction that is involved in a non-cyclic electron transfer. An important feature of the cyclic and non-cyclic fractions is that their relative amplitudes do not change under prolonged

illumination. This behavior rules out the possibility that they are due to two competing pathways since if all RCs had even a low probability for the non-cyclic pathway, prolonged illumination would lead to a complete non-cyclic charge separation.